

Comparison of atomic-level simulation methods for computing thermal conductivity

Patrick K. Schelling,^{1,2} Simon R. Phillpot,² and Pawel Keblinski³

¹*Forschungszentrum, 76021 Karlsruhe, Germany*

²*Materials Science Division, Argonne National Laboratory, Argonne, Illinois 60439*

³*Department of Materials Science and Engineering, Rensselaer Polytechnic Institute,
110 8th Street, MRC 115, Troy, New York 12180-3590*

(Received 9 July 2001; revised manuscript received 26 October 2001; published 4 April 2002)

We compare the results of equilibrium and nonequilibrium methods to compute thermal conductivity. Using Sillinger-Weber silicon as a model system, we address issues related to nonlinear response, thermal equilibration, and statistical averaging. In addition, we present an analysis of finite-size effects and demonstrate how reliable results can be obtained when using nonequilibrium methods by extrapolation to an infinite system size. For the equilibrium Green-Kubo method, we show that results for the thermal conductivity are insensitive to the choice of the definition of local energy from the many-body part of the potential. Finally, we show that the results obtained by the equilibrium and nonequilibrium methods are consistent with each other and for the case of Si are in reasonable agreement with experimental results.

DOI: 10.1103/PhysRevB.65.144306

PACS number(s): 66.70.+f, 02.70.Ns, 05.60.Cd, 44.10.+i

I. INTRODUCTION

With the dimensions of electronic and mechanical devices approaching the nanometer scale, efficient heat removal is of crucial importance to both performance and function. While a basic understanding of heat transport in dielectrics has already been achieved, many important issues remain unresolved. Interpretation of experimental results remains difficult because typically the contributions of individual defects cannot be deconvoluted. Molecular-dynamics (MD) simulations are ideal for addressing such issues since they can be used to study individual microstructural elements, thereby identifying the most important issues for thermal conductivity in polycrystalline materials. For example, by elucidating the correlation between grain-boundary structure and thermal-transport properties, one may hope to eventually design materials with tailored thermal properties. However, prior to a systematic study of interfacial effects, it is necessary to firmly establish suitable computational methods. While there are a number of studies of thermal transport in bulk or interfacial systems, methodological issues still remain unresolved. The aim of this paper is to resolve the remaining methodological issues, thereby laying a solid foundation for the simulation of heat-transfer problems in solids.

The thermal conductivity relates the heat current to the temperature gradient via Fourier's law as

$$J_{\mu} = - \sum_{\nu} \kappa_{\mu\nu} \partial T / \partial x_{\nu}, \quad (1)$$

where J_{μ} is a component of the thermal current, $\kappa_{\mu\nu}$ is an element of the thermal conductivity tensor, and $\partial T / \partial x_{\nu}$ is the gradient of the temperature T . Experimentally, κ is typically obtained by measuring the temperature gradient that results from the application of a heat current. In MD simulations the thermal conductivity can be computed either using nonequilibrium MD (NEMD)¹⁻¹¹ or equilibrium MD (EMD).^{1,12-18} The two most commonly applied methods for computing thermal conductivity are the "direct method"¹⁻⁷ and the

Green-Kubo method.^{1,12-18} The direct method is an NEMD method that relies on imposing a temperature gradient across the simulation cell¹⁻⁷ and is therefore analogous to the experimental situation. By contrast, the Green-Kubo approach is an EMD method that uses current fluctuations to compute the thermal conductivity via the fluctuation-dissipation theorem.

In this paper we systematically explore both the direct and Green-Kubo methods. In each case, we first address issues related to the simulation time necessary to achieve equilibrium or steady state and also accurate statistical averaging. We then demonstrate the importance of finite-size effects that arise when the mean free path for a bulk system is comparable to the size of the simulation cell. In the direct method we find that unless the simulation cell is many times longer than the mean-free path, scattering from the heat source and heat sink contributes more to the thermal resistivity than does the intrinsic anharmonic phonon-phonon scattering. However, we show in Sec. II that a value for the thermal conductivity of an infinite system can be reliably obtained by the direct method from simulations of different size systems and an extrapolation of the results to an infinite-size system. Finally, we compare the results of the direct and Green-Kubo methods. For thermal transport in liquids, a comparison has previously been made showing good agreement between the Green-Kubo and an NEMD method.¹⁸ However, thermal transport in liquids is very different from solids, and also the NEMD method used in Ref. 18 is different from the direct method considered here. Only one comparison of the direct method and the Green-Kubo method for determining thermal transport in solids has previously been published.⁷ This work demonstrates good agreement between the direct and Green-Kubo methods for the special case of a disordered two-dimensional lattice model; however, the system was finite and not periodically repeated, thereby introducing boundary scattering. In this paper, we simulate the more general case of three-dimensional systems with periodic-boundary conditions. By contrast with Ref. 7, the elimination of surface scattering by the application of periodic-boundary conditions results in very weak finite-size effects for the Green-Kubo method. We thus find that the finite-size effects associated with using the Green-Kubo method are actually very differ-

ent from those associated with the direct method. Nevertheless, when finite-size effects are treated correctly and sufficiently long simulations are performed, the Green-Kubo method and the direct method are indeed consistent with each other.

We use crystalline silicon as a model system for our simulations. Because Si is a semiconductor, it is expected that the contribution to heat conduction by the electrons will be small, and thus an atomistic model that ignores electron transport can be used. In addition, a very well understood potential for Si due to Stillinger and Weber (SW) already exists.¹⁹ The SW potential utilizes two- and three-body interaction terms (see below) in order to stabilize the diamond lattice. This potential accurately describes elastic properties, phonon dispersion curves, yield strengths, and thermal-expansion coefficients.^{20–23} Using the elastic constants obtained in Ref. 22 for the SW model, we compute the longitudinal and transverse acoustic sound velocities to be 8040 and 5720 m/s, which are very close to the experimental values of 8480 and 5860 m/s.²⁴ Since the thermal-transport properties of a perfect crystal are governed by the acoustic sound velocities and anharmonic effects that are also important for thermal expansion, the SW potential should be well suited to describe the thermal conductivity of Si near or above the Debye temperature, which is about 650 K.²⁴ Furthermore, much work has been done to characterize grain boundaries in Si, making it an ideal system to study grain-boundary effects.^{25,26}

The rest of the paper is organized as follows. Section II describes the direct method, including results for Si. Section III details results of the application of the Green-Kubo EMD method. In the final section, we discuss the strengths and weaknesses of the two methods, and directly compare the results obtained for the Si system under consideration.

II. DIRECT METHOD

In this section we present a brief discussion of details related to the direct method and results for the SW Si potential. In particular, we present an analysis of thermal equilibration, the effects of nonlinear response, and finite-size effects. We analyze the finite-size effects in detail, including a comparison to finite-size effects observed in simulations of diamond, and demonstrate how results for an infinite bulk system can be extrapolated in spite of the importance of the scattering that occurs at the heat source and heat sink.

A. Background

The direct method of computing the thermal conductivity is analogous to the experimental measurement. In Fig. 1 we show a schematic representation of the simulation cell used to compute κ . By rescaling particle velocities at each MD time step, heat $\Delta\epsilon$ is added in a thin slab of thickness δ centered at $z = -L_z/4$ and removed from a slab of the same thickness centered at $z = +L_z/4$. Each particle velocity in the source/sink region is scaled by the same factor such that the resulting net kinetic energy is increased/decreased by an amount $\Delta\epsilon$. Although only kinetic energy, and not potential energy, is added to the system, we expect that within a typi-

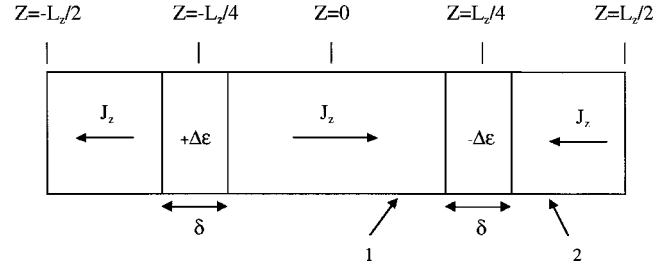


FIG. 1. Schematic representation of three-dimensional periodic simulation cell for direct summation of thermal conductivity. The simulation cell has length L_z . There is a slab of thickness δ at $z = -L_z/4$ into which energy $\Delta\epsilon$ is added at each MD step. Likewise, in the slab at $z = L_z/4$, energy $\Delta\epsilon$ is removed at each MD step. The resulting thermal current is J_z . Points labeled 1 and 2 show approximate positions of slabs used to examine evolution of the time-averaged temperature (see Fig. 2).

cal vibrational period (< 1 ps), equilibration between kinetic and potential energy will occur. Thus, when the system achieves steady state, the heat current is given by $J_z = \Delta\epsilon/2A\Delta t$. The resulting temperature gradient is then calculated, and Fourier's law [Eq. (1)] is used to obtain κ . A complication arises from the need to eliminate the tendency of the center of mass of the entire system to drift, an effect that results in an inaccurate measurement of the actual local temperature that must be defined using velocities obtained in a system with zero center-of-mass velocity. We therefore use the velocity-rescaling algorithm of Jund and Jullien⁵ that eliminates this drift. Since equal amounts of energy are added and removed at each time step, energy is conserved to better than 1 part in 10^6 for an MD step of 0.55 fs. In addition to these considerations, we shall see below that this method creates energy currents that can propagate ballistically across the system. However, by performing several simulations for different systems sizes, the behavior of an infinite system can be extrapolated.

From Fig. 1 we see that the presence of the heat source and heat sink and the application of periodic-boundary conditions produces a current in two opposite directions. Because the heat current flows along a well-defined direction in the lattice, a single simulation can be used to obtain κ only along one crystal lattice direction. To obtain κ along a different crystal lattice direction, an entirely new simulation with a different simulation cell must be performed. This limitation does not exist for the Kubo method, where the entire thermal conductivity tensor is computed in just one simulation.

The direct method involves large ($\sim 10^9$ K/m) temperature gradients. Because these temperature gradients are well outside of the experimental range, it is not clear *a priori* that results obtained using the direct method will be consistent with experiment. Specifically, very large temperature gradients may introduce significant nonlinear response effects such that Fourier's law may not apply; therefore, it is important to test the effect of changing the magnitude of the thermal current on the resulting computed value of κ . Below we shall establish that there exists a range of values for $\Delta\epsilon$ where the degree of nonlinearity is acceptable.

A critical feature of the simulation cell shown in Fig. 1 is the existence of boundaries at the edges of the heat source and heat sink. Because the atomic dynamics in the hot and cold slabs is altered by the simulation algorithm, the mean-free path is limited by the size of the system; this regime is known as the Casimir limit. The mean-free path can be estimated from data for the thermal conductivity, specific heat, and velocity of sound. As we estimate below for SW Si at 500 K, the mean-free path is about 100 nm. However, as we will demonstrate, by carrying out a finite-size analysis of significantly smaller systems, it is possible to obtain a good estimate of κ for an infinite system.

B. Equilibration

For the direct method, it is important to establish that a steady-state current flow has been achieved. This amounts to obtaining a stationary temperature profile as a function of time, thus insuring that only steady-state currents are flowing and, hence, that the thermal conductivity can be obtained from Fourier's law [Eq. (1)]. It was found by Maiti, Mahan, and Pantelides² that very long (~ 1 ns) simulations were necessary to achieve a smooth temperature profile for a Si grain-boundary system. We therefore chose a total simulation time of 1.1 ns (2×10^6 MD steps for an MD time step of 0.55 fs). We compute the average temperature in a thin slice (0.14 nm in width) of the system centered at position z as

$$\langle T(z) \rangle_M = \frac{1}{M} \sum_{m=0}^{M-1} T_{N-m}(z), \quad (2)$$

where $\langle T(z) \rangle_M$ is the average temperature at z averaged over the final M time steps of the simulation, and $T_{N-m}(z)$ is the instantaneous temperature at z for the time step $N-m$. The total number of steps in the simulation is N , and one can therefore see that M must be smaller than $N-1$. By averaging in this way, we can be certain that for small M , the fluctuations are entirely statistical and not due to transient effects related to the current sources. As M increases, we may see fluctuations due to transient effects related to achieving a steady-state thermal current. In Fig. 2 we show the time-averaged temperatures of slices 19 nm to either side of the heat sink for a $4 \times 4 \times 288$ system at 500 K (see Fig. 1 for the approximate positions of the two slices). To obtain Fig. 2, data were first averaged over 1000 MD step segments, which tends to eliminate some of the large temperature fluctuations that occur for very short times ($\ll 1$ ps). We see very little evidence of fluctuations in the averages as the averaging time is extended back near $t=0$. Apparently the system achieves steady state rather quickly so that the amount of time for which the system is not in steady state is small compared to the entire 1.1 ns simulation time. Also, this indicates that 1.1 ns is a long enough simulation time to obtain time-averaged temperature profiles, in agreement with the results of Maiti, Mahan, and Pantelides.² Even though transient effects appear to be small, in the following we throw out the initial 110 ps of simulation data to be certain that the system has reached steady state, thereby leaving 990 ps of data over which to compute time-averaged temperature

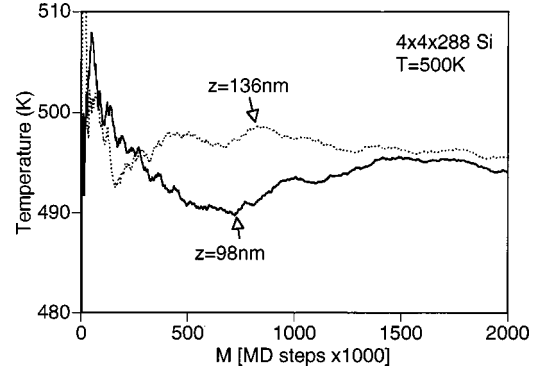


FIG. 2. Time-averaged temperature for slices at $z=136$ nm (dotted line) and $z=98$ nm (solid line) for a $4 \times 4 \times 288$ simulation cell of Si using the direct method with $\Delta \varepsilon = 5 \times 10^{-4}$ eV and an average system temperature of 500 K. These slices are both 19 nm from the heat sink, which is located at $z=117$ nm. The approximate positions of the slabs are shown in Fig. 1, with point 1 corresponding to $z=98$ nm and point 2 corresponding to $z=136$ nm. Time averages [see Eq. (2)] begin at the end of the simulation ($M=0$), and are done up to the total length of the simulation ($M=N-1$). In this figure, data were first averaged over 1000 MD step segments. The entire simulation was 2×10^6 MD steps, which corresponds to 1.1 ns.

profiles. We note that the two time-averaged temperatures shown in Fig. 2 should be the same since they are taken at equal distances from the heat sink. We find a difference of about 2 K after 1.1 ns of averaging, which we take as a measure of the statistical precision of the calculation. Typically, we find the statistical precision to be within about ± 3 K for any point along the temperature profile. This is very good precision especially considering that each 0.14 nm thick slice at a given position z contains only 32 atoms for a simulation cell 4×4 in the direction perpendicular to the thermal current.

In Fig. 3 we show a typical time-averaged temperature profile used to compute the thermal conductivity. In this case, the system dimensions are $4 \times 4 \times 288$ cells, and the average temperature is 500 K. Within 6 nm of the source or sink region, a very strong nonlinear temperature profile is observed, which has been attributed by other authors to the strong scattering caused by the heat source or heat sink.^{2,4} In the intermediate region (at least 6 nm away from the heat source and sink), the temperature profile is fit with a linear function as shown in Fig. 4; the resulting temperature gradient is used in Eq. (1) to obtain κ . We note that the gradients measured for the two different linear regions, 0.31 and 0.32 K/nm, are very similar. Typically, the gradients fit to the two linear regions differ by less than 15%. The observed differences in the computed gradients for the two different regions are used to obtain an error estimate for the value of the thermal conductivity (see Fig. 6). As we shall see below in Sec. IID, the temperature profile observed in Figs. 3 and 4 results from a partly diffusive and partly ballistic transport of energy, the latter due to the fact that the systems sizes used are comparable to the mean-free path of phonons in the system.

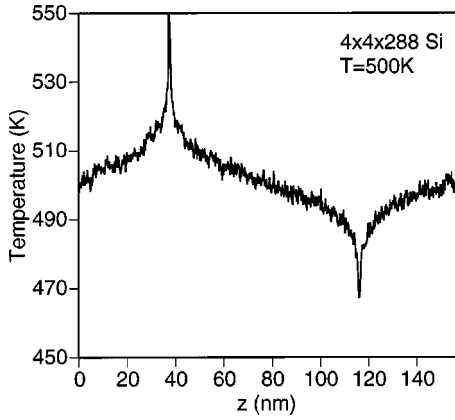


FIG. 3. Typical temperature profile for a $4 \times 4 \times 288$ system at an average temperature of 500 K. The heat source is located at $z = 39$ nm, and the heat sink is located at $z = 117$ nm. Within 6 nm of the source and sink, a strong nonlinear temperature profile is always observed. For obtaining temperature gradients to compute κ from Fourier's law [Eq. (1)], we therefore make linear fits using only parts of the system, which are at least 6 nm away from the heat source and sink (see Fig. 4).

C. Effect of deviations from Fourier's law

To establish that Fourier's law [Eq. (1)] is obeyed and that nonlinear response effects are not important, it is necessary to establish that the computed value of κ does not depend strongly on the value of $\Delta\varepsilon$ for some range of values of $\Delta\varepsilon$. To do this, we have computed κ for several different values of $\Delta\varepsilon$ for a $4 \times 4 \times 96$ system at $T = 500$ K. The thermal current is proportional to $\Delta\varepsilon/A$, where A is the cross-sectional area of the system ($A = 4.73$ nm² for the $4 \times 4 \times 96$ system). The results are shown in Fig. 5. We see that while there does appear to be some variation of κ with $\Delta\varepsilon$, for values of $\Delta\varepsilon/A$ near 1.06×10^{-4} eV/nm² (corresponding to $\Delta\varepsilon = 5 \times 10^{-4}$ eV for a system with $A = 4.73$ nm²), the variations appear to be rather small ($< 10\%$), and an accurate value of κ can be calculated. Choosing $\Delta\varepsilon/A$ significantly smaller than 1×10^{-4} eV/nm² tends to result in large error bars because the magnitude of the temperature difference between the hot and cold ends of the simulation cell becomes comparable to the typical statistical noise. Although no significant deviations from Fourier's law are apparent from Fig. 5, we will avoid unnecessarily large values of $\Delta\varepsilon/A$. Thus, choosing a value of $\Delta\varepsilon/A \sim 1 \times 10^{-4}$ eV/nm² (i.e., 1.6×10^{-5} J/m²) appears to be suitable, and in the remainder of this paper we will use a value of 5×10^{-4} eV for $\Delta\varepsilon$ for systems of dimension 4×4 (i.e., 4.73 nm²) in the direction perpendicular to the current.

D. Finite-size effects

Finite-size effects arise when the length of the simulation cell L_z is not significantly longer than the phonon mean-free path.^{4,7} This is understood to be a result of scattering that occurs at the interfaces with the heat source and sink. For a sample with length smaller than the mean-free path in an infinite system, the thermal conductivity will be limited by the system size. This regime is known as the Casimir limit. A

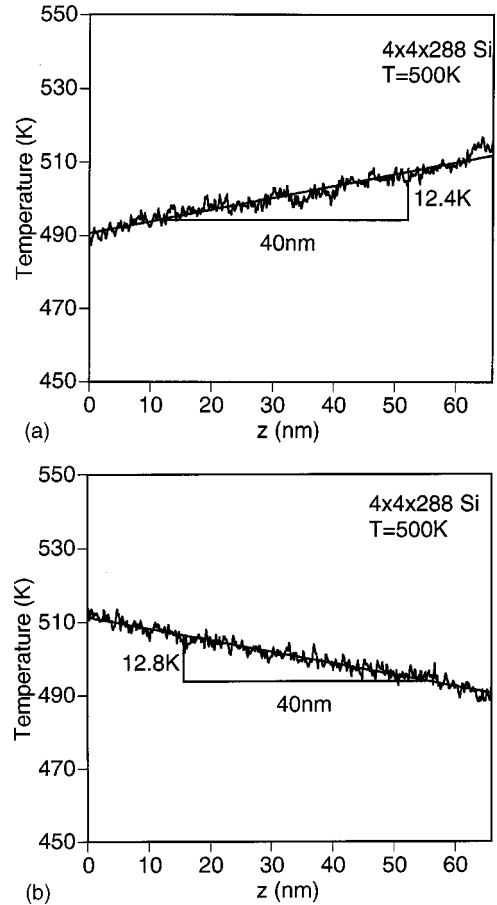


FIG. 4. Linear fits to temperature profiles for a $4 \times 4 \times 288$ system at an average temperature of 500 K (see Fig. 3). Temperature profiles were fit for the regions at least 6 nm away from the heat source. In this case, linear fits are made over 66 nm of the system. The fits in the case have slopes of (a) 0.31 K/nm and (b) 0.32 K/nm. Taking the average, this results in a thermal conductivity from Eq. (1) of 47.9 W/mK.

simple approach to determine the effective mean-free path l_{eff} when $L_z \sim l_\infty$, where l_∞ is the mean-free path for an infinite system, is to add the inverse mean-free paths. Then l_{eff} is given by,

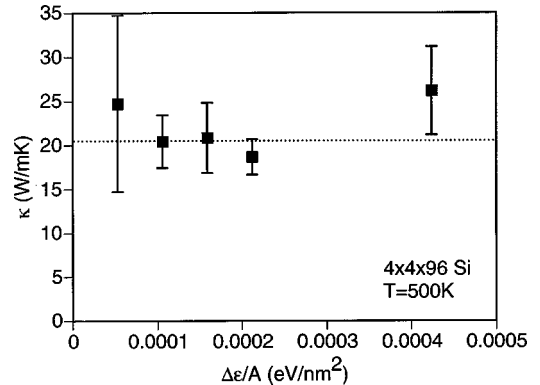


FIG. 5. Effect of changing $\Delta\varepsilon$ for a $4 \times 4 \times 96$ system at an average temperature of 500 K. This shows a broad range of values for $\Delta\varepsilon/A$ where nonlinear behavior is not present and Fourier's law is obeyed.

$$\frac{1}{l_{\text{eff}}} = \frac{1}{l_{\infty}} + \frac{4}{L_z}. \quad (3)$$

Here, the factor of 4 accounts for the fact that as phonons travel along the length of the simulation cell from the source to the sink, its *average* distance since the last scattering event should be $L_z/4$. In other words, if we randomly select several phonons, on average they will be at a distance $L_z/4$ from either the source or the sink where the last anharmonic scattering event occurred. This assumes it has not undergone any anharmonic phonon-phonon scattering in the region between the source and the sink (i.e., it moves ballistically across the system). Equation (3) suggests that a plot of $1/\kappa$ vs $1/L_z$ should be linear, and that the thermal conductivity of an infinite system can be obtained by extrapolating to $1/L_z=0$. Indeed, this procedure has been carried out by Oligschleger and Schon to obtain κ from simulations of trigonal Se crystals.⁴

In addition to ballistic phonon transport, Cenian and Gabriel²⁷ have found that solitonlike modes may propagate ballistically across a system, resulting in deviations from Fourier's law and a system-size-dependent thermal conductivity. However, these effects depend strongly on the energy of the input pulse and are only important for input energies on the order of a few eV. This can be compared to the rather small input energies used here ($\sim 10^{-4}$ eV). In the last section, we showed that the current simulation results depend only weakly on the excitation energy $\Delta\epsilon$, which is an indication that ballistic soliton propagation is not important in the current work. Even if solitons were a significant mode of energy transport in the current work, Eq. (3) should still be a useful way of determining the mean-free path for an infinite system l_{∞} as long as the system sizes used are at least comparable to l_{∞} . In Ref. 27, the soliton mean-free path was found to be about 70 lattice parameters at temperatures below 50 K and can be expected to decrease strongly with increasing temperature. Since we use rather long simulation cells (between 96 and 768 lattice parameters) and high temperatures (500 and 1000 K), we believe that we are always in a regime where L_z is significantly larger than the soliton mean-free path. Therefore, Eq. (3) should apply to the current work regardless of whether the ballistic component is phononlike or solitonlike.

For the Si system, we have performed simulations as a function of both L_z and simulation temperature T . We used systems ranging from 96 to 768 unit cells long, corresponding to L_z from 52 to 417 nm. For a nonprimitive unit cell containing eight atoms the largest system, $4 \times 4 \times 768$, contained 98 304 Si atoms. The results for the thermal conductivity are shown in Fig. 6. For comparison, we also show data that we obtained for diamond using the Tersoff potential for carbon.²⁹ We first note from Fig. 6 that the slopes of the $T=500$ K and $T=1000$ K data for Si seem to be very similar. To understand this effect, recall that the thermal conductivity in kinetic theory is given by

$$\kappa = \frac{1}{3} cvl, \quad (4)$$

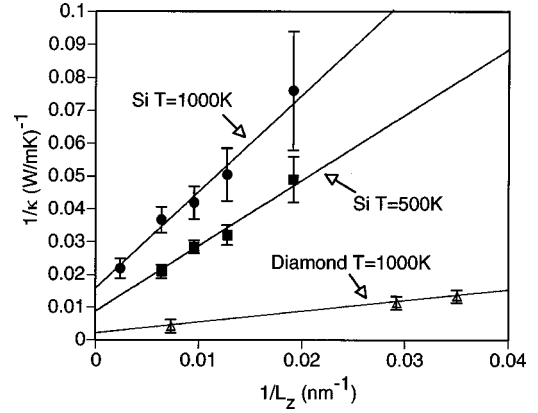


FIG. 6. System size dependence of $1/\kappa$ on $1/L_z$. Data are shown for Si at $T=500$ K and $T=1000$ K and for diamond at $T=1000$ K. We note that the rate of change of $1/\kappa$ with $1/L_z$ for Si appears to be only slightly dependent on temperature. Also, the rate of change for diamond appears to be different than the Si system. This is the result of differences in the lattice constant and sound velocities of diamond and Si.

where c is the specific heat of the phonons, v is the group velocity of an acoustic branch, and l is the mean-free path for scattering. For a purely classical simulation of the type described here, each normal mode will have $k_B T$ of energy on average. However, the specific heat in Eq. (4) is intended to be only for those that carry a significant thermal current. In the case of Si, which has three optical and three acoustic branches, we expect that the majority of heat is carried by the acoustic modes that have a significantly larger group velocity. With this assumption, the appropriate specific heat to use in Eq. (4) is given by

$$c = \frac{3}{2} k_B n, \quad (5)$$

where n is the number density of atoms in the system. Now if we use our simple approach for determining l [Eq. (3)] we obtain

$$\frac{1}{\kappa} = \frac{a^3}{4k_B v} \left(\frac{1}{l_{\infty}} + \frac{4}{L_z} \right). \quad (6)$$

This gives us a crude estimate of the slope of $1/\kappa$ vs $1/L_z$ plots shown in Fig. 6. If we assume that v in Eq. (6) is given by the average of the transverse and longitudinal branches as $v = 1/3(v_L + 2v_T)$, we obtain $v \approx 6500$ m/s from the elastic constants calculated in Ref. 21 for the SW potential. This results in a prediction of the slope of $1/\kappa$ vs $1/L_z$ for the SW Si model of 1.8×10^{-9} m²K/W, which can be compared to the result of the linear fit in Fig. 6 at 500 K of $(2.0 \pm 0.4) \times 10^{-9}$ and $(2.9 \pm .5) \times 10^{-9}$ m²K/W at 1000 K. For diamond, which has a smaller lattice constant and larger sound velocity, we see the Eq. (6) predicts a smaller slope when compared to Si, which is indeed observed in Fig. 6. Using the experimental sound velocities,²⁸ we obtain a prediction for the slope of 2.2×10^{-10} m²K/W, which can be compared to the result in Fig. 7 of $(3.3 \pm .01) \times 10^{-10}$ m²K/W. While the predictions and actual observed results appear to differ somewhat, and there appears to be some temperature depen-

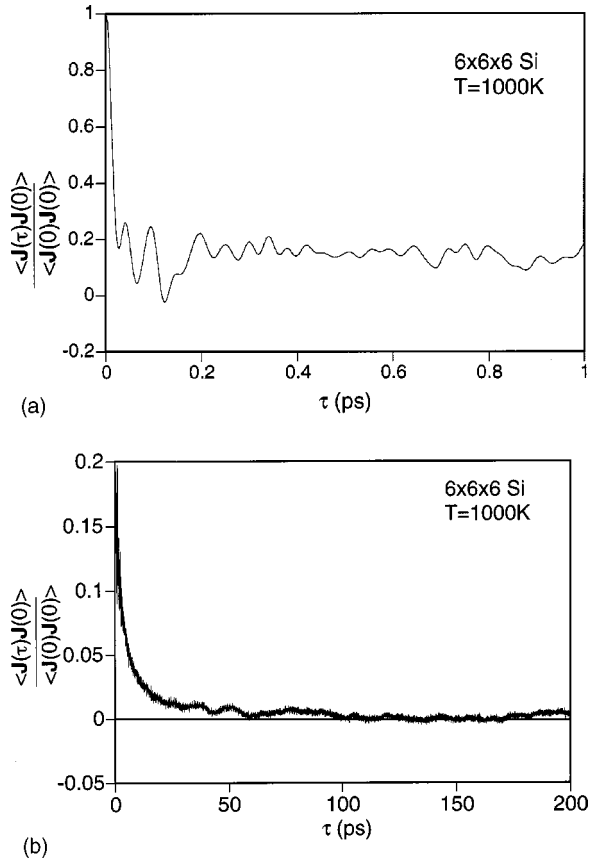


FIG. 7. Normalized current-current correlation function $\langle \mathbf{J}(\tau) \cdot \mathbf{J}(0) \rangle / \langle \mathbf{J}(0) \cdot \mathbf{J}(0) \rangle$ vs τ for a $6 \times 6 \times 6$ Si system containing a total of 1728 atoms. In (a), we see that for very short times (< 0.1 ps) there is a very abrupt decay in the current-current correlations. For longer times in (b), we see that correlations in the current persist out to 100 ps.

dence of the slope, the general trend of increasing slope with increasing lattice constant and decreasing sound velocity appears to be consistent with the predictions of Eq. (6).

The linear fits in Fig. 6 can also be used to estimate the thermal conductivity in the limit $1/L_z = 0$. For Si, $\kappa(1/L_z = 0)$ is 119 ± 40 W/mK at 500 K and 65 ± 16 W/mK at 1000 K. For natural Si, defect scattering significantly reduces κ , and the experimental values at 500 and 1000 K are about 80 and 30 W/mK, respectively.²⁴ While the experimental data for isotopically enriched Si (i.e., containing fewer defects) only extends to 375 K, the data in Ref. 30 were extrapolated to yield a value of about 120 W/mK at 500 K. At 1000 K, the observed temperature dependence of $T^{-\alpha}$ with $\alpha \approx 1.25$ can be used to obtain the much more uncertain estimate for κ of 50 W/mK.³⁰ These numbers are in reasonable agreement with the simulation results obtained using the direct method. This is not altogether surprising given the high quality of the SW potential and the fact that we are comparing results at temperatures near or above the Debye temperature [~ 650 K for Si (Ref. 30)], which is the point where a classical simulation should become valid. However, to fully compare the temperature dependence of κ , more simulations are required. We also remark that the values for α of 1.5 and 1.6 have been observed in simulation and experiment, respectively.¹⁴

TABLE I. Comparison of κ as for different cell sizes perpendicular to the direction of the current. Each system was 144 unit cells long parallel to the current. Values of $\Delta\varepsilon$ were scaled with the system size so that the resulting thermal current J_g was the same in each case. The estimated error in κ in each case is ± 3 W/mK.

Transverse dimensions	$\Delta\varepsilon$ (eV)	κ (W/mk)
2×2	1.25×10^{-4}	34
3×3	2.81×10^{-4}	29
4×4	5.00×10^{-4}	31
6×6	11.25×10^{-4}	30

For diamond at 1000 K, $\kappa(1/L_z = 0)$ is 573 ± 60 W/mK, compared to about 400 W/mK from experiment for isotopically enriched diamond.³¹ We note that small errors in the linear fits can result in rather large errors in the extrapolated value of the thermal conductivity, especially when the extrapolated value of κ is very large.

We note that Eq. (6) provides a means of predicting the system size necessary to achieve a given level of precision in computing κ via the direct method. For example, Eq. (6) implies that we require a system size ten-times longer than the mean-free path in an infinite system l_∞ , in other words $L_z \approx 40 l_\infty$, to obtain a value of κ within 10% of the correct bulk value. Using the slopes calculated above for the dependence of $1/\kappa$ on $1/L_z$ (1.8×10^{-9} m²K/W for Si and 2.2×10^{-10} m²K/W for diamond), we can estimate the mean-free paths for a bulk system l_∞ based on the extrapolated value of κ . For Si, estimating l_∞ in this way results in values of 100 nm at $T = 500$ K and 60 nm at $T = 1000$ K. For diamond we obtain 65 nm at $T = 1000$ K. These estimates suggest that we require a system at least 7300 unit cells long to obtain a result within 10% for Si at 500 K, which is almost ten-times longer than the largest system studied here. Fortunately, we have shown here that even for small systems, extrapolation to the infinite-system limit is possible, and also that useful information (for example temperature dependence of κ) can be obtained even from system with $L_z \ll l_\infty$.

We have also studied the dependence of κ on the dimensions perpendicular to the current flow. It is expected that κ will not depend as sensitively on the dimensions perpendicular to the current as on the length L_z . Due to periodic boundary conditions on the simulation cell, phonons are free to travel across the simulation cell perpendicular to the current direction without scattering from any boundaries. Hence changing the dimension perpendicular to the current does not change the scattering in any obvious way. In Table I we show a comparison of κ obtained for systems of different sizes in the direction perpendicular to the current. For each different system size we have scaled the value of $\Delta\varepsilon$ so that the resulting current density J_z is the same in each case. The different values of $\Delta\varepsilon$ used are also shown in Table I. While still equivalent within statistical uncertainties, the 2×2 system studied appears to have a value for κ slightly larger than the results for larger systems. Cells with L_z much larger than the transverse dimension will have tend to sample a larger fraction of modes with wave vector along the current direction. To estimate this effect, we note that for a finite-size

system the thermal conductivity κ can be written in terms of the cell volume Ω , group velocity v , and mean-free path l as

$$\kappa = 1/\Omega k_B v l \sum_{k_x, k_y, k_z} k_z^2 / k^2, \quad (7)$$

where the summation is over all component k_x , k_y , and k_z appropriate for the system consideration. For a very large system, the value of the summation in Eq. (7) approaches 1/3 and hence we obtain the standard result for κ given by Eq. (4). However, the summation in Eq. (7) can be different for small or irregularly shaped systems. Using Eq. (7) we estimate that this effect can produce an increase in value of the thermal conductivity for a $2 \times 2 \times 144$ system of at most 20% compared to a $4 \times 4 \times 144$ system. For system sizes of 3×3 unit cells or larger, the values of κ in Table I are equivalent within the error inherent in the calculations, and there appears to be no systematic changes in κ as the transverse dimensions are changed. These results indicate that the 4×4 systems used for Fig. 7 is adequate and that the values of $1/\kappa$ obtained by extrapolation to $1/L_z = 0$ are representative of the true infinite-system limit.

We have shown in this section that the direct method is a practical method for obtaining the thermal conductivity of bulk materials. Deviations from Fourier's law appear to be small over a large range of values for $\Delta\varepsilon$. Also, we have found that 1 ns of simulation time is adequate to obtain smooth temperature profiles. Most importantly, we have shown how to estimate finite-size effects related to the length L_z and also how to extrapolate results to the infinite limit ($1/L_z = 0$). Finally, finite-size effects related to the dimensions perpendicular to the applied current appear to be small.

III. GREEN-KUBO METHOD

The Green-Kubo method represents an EMD technique to compute κ . Because simulations are done in equilibrium, and the transport coefficients ascertained using the Green-Kubo formula as a result of the fluctuation-dissipation theorem, there is no imposed driving force, and hence the system is always in the linear-response regime. However, it has been established that finite-size effects do play a role in applying the Green-Kubo method.^{12,14} In addition, very long simulation times appear to be needed to sufficiently converge the current-current autocorrelation function (see below).^{12,13,16} In this section we use the Kubo method to compute κ for Si. We address the finite-size effects as well as convergence difficulties due to the finite simulation time.

A. Background

EMD simulations rely on relating the equilibrium current-current autocorrelation function to the thermal conductivity via the Green-Kubo expression

$$\kappa_{\mu\nu}(\tau_m) = \frac{1}{\Omega k_B T^2} \int_0^{\tau_m} \langle J_\mu(\tau) J_\nu(0) \rangle d\tau, \quad (8)$$

where Ω is the system volume, k_B is the Boltzmann constant, T is the system temperature, and the angular brackets denote

an ensemble average, or, in the case of an MD simulation, an average over time. In practice, at each MD step we compute the heat current that is then saved to disk. Since the simulation is performed for discrete MD steps of length Δt , Eq. (8) is in fact a summation. Including the time averaging, what we actually compute is

$$\kappa_{\mu\nu}(\tau_M) = \frac{\Delta t}{\Omega k_B T^2} \sum_{m=1}^M (N-m)^{-1} \sum_{n=1}^{N-m} J_\mu(m+n) J_\nu(n), \quad (9)$$

where τ_M is given by $M\Delta t$ and $J_\mu(m+n)$ is the μ th component of the heat current at MD timestep $m+n$. Note that the number of steps for integration M must be less than the total number of simulation steps N . Typically, as we will see below, the total number of integration steps M is considerably smaller than the total number of MD steps to assure good statistical averaging. For example, the simulations presented here have N of at least 6×10^6 MD steps (3.3 ns for a 0.55 fs MD step), while the summation limit M in Eq. (9) is usually done for only about 4×10^5 MD steps ($\tau_M = 220$ ps). The bulk thermal conductivity, which is formally found from the limit $\tau_M \rightarrow \infty$, should be recovered by Eq. (9) as long as τ_M is longer than the time required for current-current correlations to decay to zero.

An important issue associated with the Green-Kubo method is the precise definition of the local energy needed to evaluate the heat current. The heat current is written as

$$\mathbf{J} = \frac{d}{dt} \sum_i \mathbf{r}_i(t) \varepsilon_i(t), \quad (10)$$

where $\mathbf{r}_i(t)$ is the time-dependent coordinate of atom i and $\varepsilon_i(t)$ is the site energy. For a pair potential, where the total potential E_{pot} energy is written in terms of the pairwise interactions $u_2(r)$ as

$$E_{\text{pot}} = \frac{1}{2} \sum_{ij} u_2(r_{ij}), \quad (11)$$

a sensible choice is to evenly divide the potential energy between each pair of atoms. Then the site energy ε_i is take to be

$$\varepsilon_i = \frac{1}{2} m_i \mathbf{v}_i^2 + \frac{1}{2} \sum_j u_2(r_{ij}). \quad (12)$$

For this definition the thermal current can easily be shown to be given by

$$\mathbf{J}(t) = \sum_i \mathbf{v}_i \varepsilon_i + \frac{1}{2} \sum_{ij, i \neq j} \mathbf{r}_{ij} (\mathbf{F}_{ij} \cdot \mathbf{v}_i), \quad (13)$$

where \mathbf{F}_{ij} is the force on atom i due to its neighbor j from the pair potential. However, the SW potential is made up of not only pairwise terms but also three-body interaction terms. While no choice is unique even for a pair potential, the choice above seems the most reasonable. For the three-body interactions, however, more than one reasonable choice is possible. The potential energy for the SW potential is written as

$$E_{\text{pot}} = \frac{1}{2} \sum_{ij} u_2(r_{ij}) + \frac{1}{6} \sum_{ijk} u_3(\mathbf{r}_i, \mathbf{r}_j, \mathbf{r}_k). \quad (14)$$

The first term is just the pair potential, which we treat as discussed above. The three-body term in the SW model is written as

$$u_3(\mathbf{r}_i, \mathbf{r}_j, \mathbf{r}_k) = \varepsilon f_3(\mathbf{r}_i/\sigma, \mathbf{r}_j/\sigma, \mathbf{r}_k/\sigma), \quad (15)$$

and the term $f_3(\mathbf{r}_i/\sigma, \mathbf{r}_j/\sigma, \mathbf{r}_k/\sigma)$ is taken to be

$$f_3(\mathbf{r}_i/\sigma, \mathbf{r}_j/\sigma, \mathbf{r}_k/\sigma) = h(r_{ij}, r_{ik}, \theta_{jik}) + h(r_{jk}, r_{ji}, \theta_{kji}) \\ + h(r_{ki}, r_{kj}, \theta_{ikj}), \quad (16)$$

where θ_{jik} is the angle between \mathbf{r}_{ij} and \mathbf{r}_{ik} . One obvious choice is to define the site energy of atom i as

$$\varepsilon_i = \frac{1}{2} m_i v_i^2 + \frac{1}{2} \sum_j u_2(r_{ij}) + \frac{1}{6} \sum_{jk} u_3(\mathbf{r}_i, \mathbf{r}_j, \mathbf{r}_k). \quad (17)$$

It can easily be seen that by summing this expression over i one obtains the kinetic energy plus the potential-energy expression for the SW potential in Eq. (14). This definition leads to a thermal current defined by

$$\mathbf{J}(t) = \sum_i \mathbf{v}_i \varepsilon_i + \frac{1}{2} \sum_{ij, i \neq j} \mathbf{r}_{ij} (\mathbf{F}_{ij} \cdot \mathbf{v}_i) + \frac{1}{6} \sum_{ijk} (\mathbf{r}_{ij} + \mathbf{r}_{ik}) \\ \times (\mathbf{F}_{ijk} \cdot \mathbf{v}_i), \quad (18)$$

where \mathbf{F}_{ij} is the force due to the pair potential and the three-body force term \mathbf{F}_{ijk} is given by

$$\mathbf{F}_{ijk} = -\nabla_i u_3(\mathbf{r}_i, \mathbf{r}_j, \mathbf{r}_k). \quad (19)$$

However, another reasonable definition is to assign terms with atom i at the vertex of the trio ijk entirely to atom i . This would then result in a definition for the local site energy of

$$\varepsilon_i = \frac{1}{2} m_i v_i^2 + \frac{1}{2} \sum_j u_2(r_{ij}) + \frac{1}{2} \varepsilon \sum_{jk} h(r_{ij}, r_{ik}, \theta_{jik}), \quad (20)$$

which leads to the expression for the heat current

$$\mathbf{J}(t) = \sum_i \mathbf{v}_i \varepsilon_i + \frac{1}{2} \sum_{ij, i \neq j} \mathbf{r}_{ij} (\mathbf{F}_{ij} \cdot \mathbf{v}_i) + \sum_{ijk} \mathbf{r}_{ij} [\mathbf{F}_j(ijk) \cdot \mathbf{v}_j], \quad (21)$$

with the three-body term $\mathbf{F}_j(ijk)$ given by

$$\mathbf{F}_j(ijk) = -\varepsilon \nabla_j h_3(r_{ij}, r_{jk}, \theta_{jik}). \quad (22)$$

It has been assumed that the exact definition of the local site energy ε_i is not crucial to the results for the heat current. However, to the best of our knowledge this assumption has never been tested. To investigate this point, we have compared the thermal conductivity obtained from Eqs. (17)–(19) to Eqs. (20)–(22). These results are presented below.

One advantage of using the Green-Kubo method is that it easily permits the study of anisotropic effects in the thermal conductivity. This is not easily accomplished with the direct method described above since one picks a direction and im-

poses a thermal current. The Green-Kubo method can compute the entire thermal conductivity tensor with only one simulation, and by a simple rotation obtain the thermal conductivity along any crystal direction. However, for a cubic system like the one considered here, κ is known to be isotropic.

In order to preserve the underlying cubic symmetry due to the cubic diamond lattice, we use cubic supercells in our simulations. We chose a simulation cell with the x , y , and z axes placed along the [100], [010], and [001] crystal directions, respectively. With this orientation, the diagonal elements ($\mu = \nu$) of the thermal conductivity tensor defined by Eq. (8) should be identical. Likewise, the off-diagonal elements ($\mu \neq \nu$) in Eq. (8) should all be zero.

B. Equilibration and statistical averaging

The Green-Kubo expression is found to converge very slowly, and direct integration apparently can lead to ambiguous results.^{12–16} To obtain reliable results by direct integration a very large number of MD steps N must be used for accurate statistical averaging [see Eq. (9)]. In addition, the number of integration steps M [see Eq. (9)] must be chosen so that the integration time τ_M is larger than the characteristic time required for the current-current autocorrelation function to decay to zero. We shall see in this section that these requirements result in a total simulation time greater than 1 ns and an integration time τ_M of at least 200 ps.

To help reduce the total length of a MD simulation needed to obtain κ , often the results for the current-current autocorrelation function are fit to an exponential function of τ , which is then integrated.^{12,13,16} The idea is to fit the exponential to data for small times ($\tau < 10$ ps) where good statistical averaging is relatively easy to obtain. A second technique¹³ to reduce the necessary computational load is to apply Fourier transformations to the current, and then take the limit $\omega \rightarrow 0$ of the expression

$$\kappa_{\mu\nu}(\omega, T) = \frac{1}{\Omega k_B T^2} J_\mu(\omega) J_\nu^*(\omega). \quad (23)$$

However, because the simulation time is finite, the averaging used to obtain $\mathbf{J}(\omega)$ may not be reliable for low frequencies, and hence the $\omega \rightarrow 0$ limit is not trivial to perform.^{13,15} Both techniques rely on assuming an exponential decay of the current-current autocorrelation function. By performing very long simulations (> 3 ns), we show below that the decay of the current-current autocorrelation function is not exponential, and hence neither exponential fitting nor extrapolation of Eq. (23) to $\omega \rightarrow 0$ represents a reliable way to obtain κ .

In Fig. 7 we show a typical current-current autocorrelation function vs τ [see Eq. (8)] for a $6 \times 6 \times 6$ diamond system consisting of 1728 atoms averaged over the [100], [010], and [001] directions and normalized to the value at $\tau = 0$. In other words, we show in Fig. 7 the time dependence of

$$\frac{\langle \mathbf{J}(\tau) \cdot \mathbf{J}(0) \rangle}{\langle \mathbf{J}(0) \cdot \mathbf{J}(0) \rangle} = \frac{\sum_{\mu=1}^3 \langle J_\mu(\tau) J_\mu(0) \rangle}{\sum_{\mu=1}^3 \langle J_\mu(0) J_\mu(0) \rangle} \quad (24)$$

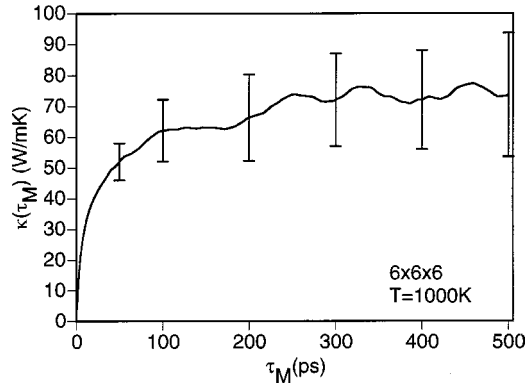


FIG. 8. Thermal conductivity at $T=1000$ K for a $6 \times 6 \times 6$ Si system found by integrating the current-current correlation function shown in Fig. 8 using Eq. (9) as a function of the upper integration limit τ_M . We see that the integral changes only very little beyond 200 ps, consistent with the observation that the current-current correlations shown in Fig. 8 are negligible beyond 200 ps.

obtained from 6 ns of total simulation time, and using the definitions of current and local energy given in Eqs. (17)–(19). We see in Fig. 7(a) that for short times ($\tau < 0.1$ ps) the autocorrelation function shows an abrupt decrease. This has also been found by Che *et al.*¹² for simulations of diamond, and is believed to be related to high-frequency optical modes that contribute little to the thermal conductivity. Indeed, it was established by Ladd, Moran, and Hoover¹⁷ that the short-time decays and oscillations found in the current-current correlations when the current is given by Eq. (10) disappear when using an alternate form of Eq. (10), which instead uses phonon occupation numbers and group velocities. For longer times, Fig. 7(b) shows that the decay appears to be much slower. As was found by Che *et al.*,¹² we find that this slow decay is most important for establishing the thermal conductivity. We note that some correlations appear to persist out to 100 ps or longer.

We obtain the thermal conductivity from Eq. (9). The value of the summation defined by Eq. (9) as a function of the integration time τ_M is shown in Fig. 8 for the same data shown in Fig. 7. At a few typical points in Fig. 9 error bars are included to show uncertainty in the results of direct inte-

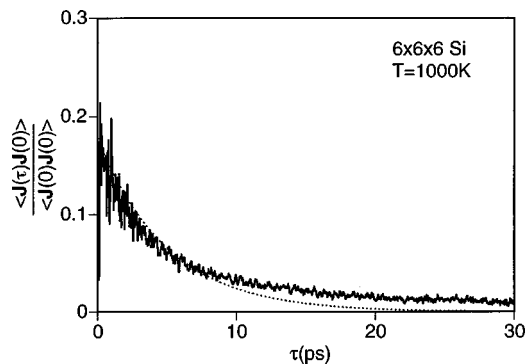


FIG. 9. Normalized current-current autocorrelation function (solid line) for the same system as in Fig. 8. Included is an exponential fit with a decay constant of 5 ps (dotted line). Beyond 10 ps, the exponential fit is very poor.

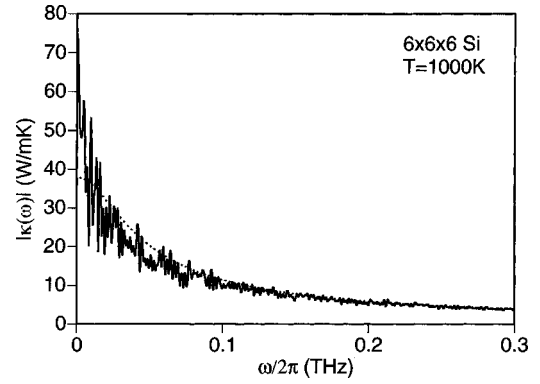


FIG. 10. Modulus of the frequency-dependent thermal conductivity vs frequency for the $6 \times 6 \times 6$ Si system at $T=1000$ K (solid line). Included is the modulus of the Fourier-transformed exponential fit (dotted line) from Fig. 10. For frequencies about 0.1 THz, the fit agrees well with the data. However, below 0.1 THz significant differences are apparent, consistent with the observation in Fig. 10 that the decay is not well fit by an exponential.

gration. The statistical error was estimated from the calculated values of κ averaged over six different 1.0 ns of data. We note that 100 to 200 ps of integration time appears to be adequate to obtain a converged value of κ , consistent with the observations above that the correlation function in Fig. 7 is very nearly zero by 100 ps. Direct integration to 200 ps in this case results in a value of 66 W/mK. For comparison, integration out to a time of 500 ps results in a value of 74 W/mK, but with significantly larger statistical error. Other simulations for different system sizes (see next section) show no systematic variation in the values of κ obtained for integration times τ_M longer than about 200 ps. Since the fluctuations in κ obtained for τ_M greater than 200 ps appear to be no larger than the estimated statistical error, we conclude that 200 ps represents an adequate integration time τ_M and that any observed fluctuations in κ for longer integration times τ_M result from statistical error.

This analysis shows that for a sufficiently long τ_M and total simulation time, direct integration can be used to obtain κ . However, it is desirable to find a technique that reduces the requirements for the total simulation time and also decreases the statistical error associated with direct integration to long times τ_M . As we noted above, one possible technique is to fit exponential decays to the simulation data that can then be integrated in Eq. (8).^{12,13,16} An example of an exponential fit to the simulation data is shown in Fig. 9 for the $6 \times 6 \times 6$ simulation. The fit exponential decay constant was 5 ps. This can be compared to about a value of about 16 ps obtained by Che and co-workers for diamond at 300 K.¹² We see in Fig. 9 that while the fit is reasonable to a time of 10 ps, for times beyond 10 ps the fit systematically underestimates the current-current correlation function. As a result, integration of the fit function results in a value for κ of 38 W/mK, significantly smaller than the direct integration result of 66 W/mK for $\tau_M=200$ ps.

In Fig. 10 we show the modulus of the frequency-dependent thermal conductivity $|\kappa(\omega)|$ along with the frequency dependence of the exponential fit shown from Fig. 9.

For exponential decays, the modulus of the frequency dependent thermal conductivity takes the form

$$|\kappa(\omega)| = \frac{\kappa(0)}{\sqrt{\omega^2 \tau^2 + 1}}, \quad (25)$$

where $\kappa(0)$ is the static thermal conductivity and τ is the decay constant that is 5 ps from the fit in Fig. 9. Above 0.1 THz the fit agrees well with the data. However, significant differences arise below 0.1 THz. This is consistent with the results of the exponential fitting in Fig. 9, which shows that only for very short times (<10 ps) does the exponential fit agree with the data.

We note that other authors have found a similar nonexponential character to the decay of the current-current autocorrelation function. For example, Volz and Chen¹⁴ found deviations in fits to the frequency-dependent thermal conductivity very similar to those shown in Fig. 10. In addition, Li and co-workers¹³ used exponential fits that appear to systematically underestimate the current-current autocorrelation function except in the regime where the function was fit. We thus conclude that the method of exponential fitting is not an accurate way to compute κ . Likewise, fitting to frequency-dependent data in Fig. 10 with a functional form given by Eq. (25) is equally undesirable.

In conclusion, we have found that 6 ns of data are adequate to obtain κ by direct integration to statistical errors within 20%. In the next section, we will use somewhat shorter simulation times (3 to 4 ns), with only slightly larger errors. Exponential fitting to current-current correlation functions, or fitting to the frequency-dependent thermal conductivity assuming an exponential decay in the current-current autocorrelation function, appears to be unjustified.

C. Finite-size effects

Finite-size effects have been seen by other authors for perfect-crystal systems when using the Green-Kubo method.^{12,14} However, because a heat source and sink are not used in the Green-Kubo method, the effect is apparently much less severe than that for the direct method. For example, Che and co-workers¹² have found in applying the Kubo formula to diamond that well converged results could be obtained for a system of only about 4000 atoms with a dimension of only 2.8 nm, much smaller than the estimated mean-free path of 174 nm. By contrast, we found above that even when the mean-free path was comparable to the system size, the direct method was different from the infinite size limit by about a factor of two. Other authors have attributed finite-size effects found using the Green-Kubo method to memory effects.¹² In this explanation, due to the periodic boundary conditions, a phonon may pass the same point in space several times without scattering. Since the system may retain some dynamical information during the passage of the phonon, artificial correlations may exist in the autocorrelation function. In this case, the correlation function may not be reliable for times longer than the time required for passage of the phonon across the simulation cell.¹²

TABLE II. Dependence of κ on system size using the Green-Kubo method with definitions provided by Eqs. (17)–(19) and Eqs. (20)–(22). The system temperature was 1000 K. System length L was obtained using the lattice constant of 0.543 nm for Si.

Dimensions	L (nm)	Number of atoms	κ (W/mK) from Eqs. (17)–(19)	κ (W/mK) from Eqs. (20)–(22)
$4 \times 4 \times 4$	2.17	512	22	22
$5 \times 5 \times 5$	2.72	1000	82	90
$6 \times 6 \times 6$	3.26	1728	66	66
$8 \times 8 \times 8$	4.34	4096	62	61

We have computed the thermal conductivity of Si using cubic cells containing 512, 1000, 1728, and 4096 atoms, all at a temperature of 1000 K. These systems correspond to lengths L of 2.17, 2.72, 3.26, and 4.34 nm respectively. For all but the 1728 atom simulation, we obtained between 3.3 and 4.1 ns of data. The 1728 atom simulation was described above and had a total of 6 ns of data. In Table II we show the computed thermal conductivity obtained by direct integration over 200 ps of the current-current autocorrelation function for different choices of simulation cell. We see that the 512 atom ($L=2.17$ nm) system results in the drastically lower value of 22 W/mK compared to the simulations at larger system size. However, it is apparent from Table II that the results for κ are well converged by 1728 atoms. This can be compared to Che *et al.*¹² for diamond, where 4096 atom system was considered adequate to obtain a converged value of κ . We note that the difference between the minimum system size required for convergence in diamond at 300 K and Si at 1000 K is likely to be due to the fact that the estimated mean-free path for diamond [174 nm at 300 K (Ref. 11)] is much larger than the mean-free path of Si (60 nm at 1000 K from estimates above).

D. Dependence on definition of local energy

The above results for the Kubo method were obtained using the definitions for the thermal current given by Eqs. (17)–(19). As we pointed out, an alternate and no less reasonable definition can be given by Eqs. (20)–(22). While no definition is unique, the two presented above are extremes in reasonable definitions, and agreement between the two different definitions would seem to suggest that results for κ are insensitive to the particular definition used.

A comparison of the results using the two definitions for the heat current is shown in Table II. The results are encouragingly similar. The biggest difference occurred in the $5 \times 5 \times 5$ cell simulation, but was still less than 10% of the magnitude of κ . It seems thus that results for κ are relatively insensitive to the particular definition of the thermal current, and the fact that there is no rigorous and unique definition for the thermal current is not a serious impediment to using the Green-Kubo method.

IV. DISCUSSION AND CONCLUSIONS

Having computed the thermal conductivity of Si using the direct method and the Green-Kubo method, we are now in a

position to directly compare the results. For the direct method at 1000 K, extrapolation to $1/L_z=0$ yields a value of κ of 65 ± 16 W/mK. The Green-Kubo method gives a result of 62 ± 16 W/mK for an $8 \times 8 \times 8$ system at 1000 K. We thus see that the two different methods yield essentially the same result within the errors inherent in the two different calculations. Furthermore, both methods are in reasonable agreement with the extrapolated experimental value of about 50 W/mK at 1000 K.³⁰ This is good evidence that either method can be applied to compute bulk thermal conductivity in perfect crystalline solids.

We also found nonexponential decays of the autocorrelation function. Fitting to the autocorrelation function or the frequency-dependent thermal conductivity assuming exponential decays resulted in various estimates of κ , which differed by as much as a factor of 2 from direct integration of the autocorrelation function and from results of the direct method. Thus, although the error bars obtained in the calculations reported here are rather large, we believe that the results obtained by direct integration of the autocorrelation function represents the most reliable way to compute κ when using the Green-Kubo method.

Each method apparently has its own strengths and weaknesses. For the direct method, the use of large temperature gradients required ($\sim 10^9$ K/m) could introduce significant nonlinear effects; however, the results of Sec. II indicate that nonlinear effects are small in this regime of temperature gradients. For the Green-Kubo method, by contrast, one is always assured of being in the linear-response regime. The issue of simulation time appears to be a more significant consideration for the Green-Kubo method, where very slow convergence of the current-current correlation function is observed. For example, while ~ 1 ns of time appears adequate to obtain a smooth temperature profile and a value for κ converged to within $\pm 10\%$ using the direct method, the same amount of simulation time using the Kubo method results in statistical errors as large as $\pm 50\%$.

Both methods exhibit finite-size effects. These are much more severe in the direct method due to the presence of real interfaces at the heat source and sink. For a system with a long mean-free path, such as the diamond or Si systems studied here, the necessary system size to achieve a fully converged value of κ may be beyond reach of an atomistic simulation. For example, a cell of about 10^5 atoms was needed for Si at 1000 K to achieve a result within 30% of the bulk thermal conductivity. In spite of this restriction, we demonstrated how finite-size effects may be estimated before a simulation, and also how to extrapolate results to the bulk limit. However, this method requires several simulations at different system sizes in order to obtain the necessary linear fit to extrapolate to $1/L_z=0$.

In consideration of these facts, it appears that the Green-Kubo method is desirable for perfect crystal systems like Si that have a very long mean-free path. To achieve comparable levels of precision, at least ten times as much simulation was required for the direct method compared to the Green-Kubo method, mainly due to the requirement that very large cells are needed to accurately extrapolate to the infinite limit. However, we expect that very much depends on the mean-free path of the system under consideration. For example, simulations on bulk yttria-stabilized zirconia systems indicate only a very small finite-size effect due to the very small mean-free path inherent to highly defective crystals.⁸ In this case, only rather small systems sizes ($L_z \sim 20$ nm) are required by the direct method. We expect that in this case the direct method will be computationally more efficient although we have not directly tested this point.

For an inhomogeneous system containing, for example, a grain boundary, the direct method is preferable because it is possible to directly compute the Kapitza resistance.^{2,28} By contrast, the Kubo method simply computes an average thermal conductivity over the entire system, thus rendering it unsuitable to study interfacial effects. In fact, the Green-Kubo formalism assumes that the spatial variation of an applied current must be equivalent to the spatial variation of the temperature gradient, a condition certainly not met by an inhomogeneous system. This suggests that further work needs to be done to establish whether or not Green-Kubo method can be applied at all to inhomogeneous systems. In addition, preliminary work on grain-boundary systems suggests that grain-boundary effects are typically not strongly system size dependent. This indicates that only one simulation is required to study the effect of boundary scattering when using the direct method, thereby greatly reducing the computational cost.³²

Although not a subject of the current paper, the method of Evans^{8,9} has been found by many authors to be a fast and reliable way of obtaining thermal conductivity values. By combining elements of equilibrium and nonequilibrium simulations, this method reduces the necessary computation time for obtaining κ . In addition, it may be more well suited than the Green-Kubo method for obtaining κ in the limit of $\omega=0$. As with Green-Kubo method, this method is only well suited to the describe the properties of homogeneous systems.

ACKNOWLEDGMENTS

We are grateful to Dieter Wolf for suggesting this project and for useful comments. This work was supported by U.S. Department of Energy, Office of Science under Contract W-31-109-Eng-38.

¹W. G. Hoover, *Computational Statistical Mechanics* (Elsevier, Amsterdam, 1991).

²A. Maiti, G. D. Mahan, and S. T. Pantelides, *Solid State Commun.* **102**, 517 (1997).

³P. K. Schelling and S. R. Phillpot, *J. Am. Ceram. Soc.* **84**, 2997 (2001).

⁴C. Oligschleger and J. C. Schon, *Phys. Rev. B* **59**, 4125 (1999).

⁵P. Jund and R. Jullien, *Phys. Rev. B* **59**, 13 707 (1999).

- ⁶A. Baranyai, Phys. Rev. E **54**, 6911 (1996).
- ⁷R. H. H. Poetzsch and H. Bottger, Phys. Rev. B **50**, 15 757 (1994).
- ⁸D. J. Evans, Phys. Lett. **91A**, 457 (1982).
- ⁹M. J. Gillan and M. Dixon, J. Phys. C **16**, 869 (1983).
- ¹⁰S. Berber, Y.-K. Kwon, and D. Tomanek, Phys. Rev. Lett. **84**, 4613 (2000).
- ¹¹G. V. Paolini, G. Ciccotti, and C. Massobrio, Phys. Rev. A **34**, 1355 (1986).
- ¹²J. Che, T. Cagin, W. Deng, and W. A. Goddard, J. Chem. Phys. **113**, 6888 (2000).
- ¹³J. Li, L. Porter, and S. Yip, J. Nucl. Mater. **255**, 139 (1998).
- ¹⁴S. G. Volz and G. Chen, Phys. Rev. B **61**, 2651 (2000).
- ¹⁵Y. H. Lee, R. Biswas, C. M. Soukoulis, C. Z. Wang, C. T. Chan, and K. M. Ho, Phys. Rev. B **43**, 6573 (1991).
- ¹⁶J. Che, T. Cagin, and W. A. Goddard III, Nanotechnology **11**, 65 (2000).
- ¹⁷A. J. C. Ladd, B. Moran, and W. G. Hoover, Phys. Rev. B **34**, 5058 (1986).
- ¹⁸R. Vogelsang, C. Hoheisel, and G. Ciccotti, J. Chem. Phys. **86**, 6371 (1987).
- ¹⁹F. H. Stillinger and T. A. Weber, Phys. Rev. B **31**, 5262 (1985).
- ²⁰S. J. Cook and P. Clancy, Phys. Rev. B **47**, 7686 (1993).
- ²¹J. Q. Broughton and X. P. Li, Phys. Rev. B **35**, 9120 (1987).
- ²²M. D. Kluge, J. R. Ray, and A. Rahman, J. Chem. Phys. **85**, 4028 (1986).
- ²³J. S. Kallman, W. G. Hoover, C. G. Hoover, A. J. DeGroot, S. M. Lee, and F. Wooten, Phys. Rev. B **47**, 7705 (1993).
- ²⁴M. G. Holland, Phys. Rev. **132**, 2461 (1963).
- ²⁵P. Keblinski, S. R. Phillpot, D. Wolf, and H. Gleiter, J. Am. Ceram. Soc. **80**, 717 (1997).
- ²⁶P. Keblinski, D. Wolf, S. R. Phillpot, and H. Gleiter, J. Mater. Res. **13**, 2077 (1998).
- ²⁷A. Cenan and H. Gabriel, J. Phys.: Condens. Matter **13**, 4323 (2001).
- ²⁸E. T. Schwartz and R. O. Pohl, Rev. Mod. Phys. **61**, 605 (1989).
- ²⁹J. Tersoff, Phys. Rev. B **39**, 5566 (1989).
- ³⁰W. S. Capinski, H. J. Maris, E. Bauser, I. Sillier, M. Asen-Palmer, T. Ruf, M. Cardona, and E. Gmelin, Appl. Phys. Lett. **71**, 2109 (1997).
- ³¹L. Wei, P. K. Kuo, R. L. Thomas, T. R. Anthony, and W. F. Banholzer, Phys. Rev. Lett. **70**, 3764 (1993).
- ³²P. K. Schelling, S. R. Phillpot, and P. Keblinski (to be published).